AD-A174 684 EXTERNAL NONLINEAR FOCUSING AND ITS APPLICATION TO ULTRAFAST OPTICAL POWER LIMITING(U) MATERIALS RESEARCH LABS ASCOT VALE (AUSTRALIA) J A HERMANN ET AL. AUG 86 1/1

UNCLASSIFIED MRL-R-1013 F/G 20/5 NL

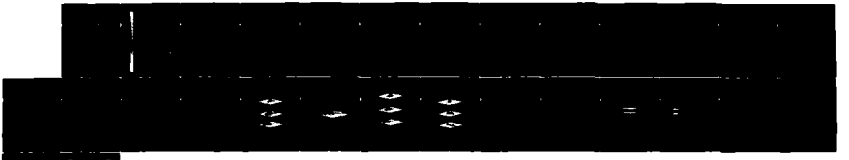

END

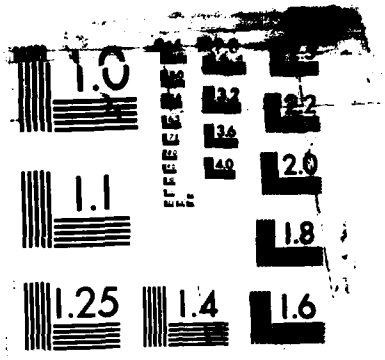

MRL-R-1013

AR-004-829

DEPARTMENT OF DEFENCE

DEFENCE SCIENCE AND TECHNOLOGY ORGANISATION

MATERIALS RESEARCH LABORATORIES

MELBOURNE, VICTORIA

REPORT

MRL-R-1013

EXTERNAL NONLINEAR FOCUSING AND ITS APPLICATION TO ULTRAFAST OPTICAL POWER LIMITING

J.A. Hermann and S.R. Kennett

DEPARTMENT OF DEFENCE

MATERIALS RESEARCH LABORATORIES

REPORT

MRL-R-1013

EXTERNAL NONLINEAR FOCUSING AND ITS APPLICATION TO ULTRAFAST OPTICAL POWER LIMITING

J.A. Hermann and S.R. Kennett

ABSTRACT

A simple model for external self-focusing or defocusing of a laser beam by a thin nonlinear phase corrector has been explored by numerical computation and by mathematical analysis.

Utilising the mechanisms of nonlinear absorption and refraction, it is shown how a passive and ultrafast power- or energy-limiting device can be constructed, with the ultimate aim of protecting optical or infrared equipment from excessive laser powers.

POSTAL ADDRESS: Director, Materials Research Laboratories
P.O. Box 50, Ascot Vale, Victoria 3032, Australia

SECURITY CLASSIFICATION OF THIS PAGE **UNCLASSIFIED**

DOCUMENT CONTROL DATA SHEET

REPORT NO.	AR NO.	REPORT SECURITY CLASSIFICATION
MRL-R-1013	AR-004-829	Unclassified

TITLE

External nonlinear focusing and its application to ultrafast optical power limiting

AUTHOR(S)

J.A. Hermann and
S.R. Kennett

CORPORATE AUTHOR

Materials Research Laboratories
PO Box 50,
Ascot Vale, Victoria 3032

REPORT DATE	TASK NO.	SPONSOR
August 1986	DST 95/117	DSTO

FILE NO.	REFERENCES	PAGES
G6/4/8-3046	22	26

CLASSIFICATION/LIMITATION REVIEW DATE	CLASSIFICATION/RELEASE AUTHORITY
August 1989	Superintendent, MRL Physics Division

SECONDARY DISTRIBUTION

Approved for Public Release

ANNOUNCEMENT

Announcement of this report is unlimited

KEYWORDS

Laser beams	Optical phase correction
Power limiting	Nonlinear focusing

COSATI GROUPS 2005

ABSTRACT

A simple model for external self-focusing or defocusing of a laser beam by a thin nonlinear phase corrector has been explored by numerical computation and by mathematical analysis.

Utilising the mechanisms of nonlinear absorption and refraction, it is shown how a passive and ultrafast power- or energy-limiting device can be constructed, with the ultimate aim of protecting optical or infrared equipment from excessive laser powers.

C O N T E N T S

EXTERNAL NONLINEAR FOCUSING AND ITS APPLICATION TO ULTRAFAST OPTICAL POWER LIMITING

1. INTRODUCTION

If a laser beam of sufficient power P_i passes through a thin nonlinear medium it will suffer an optical phase shift. In particular, when a laser beam of gaussian cross-section interacts with a refractive nonlinearity, the resultant phase shift is found [1-3] to generate strong interference effects in the external far field. The transverse profile in the far-field then consists of a set of concentric rings whose number increases with beam power (Miller et al [1], Weaire et al [2], Miller et al [3]). The present report studies the power-limiting capability of a thin nonlinear medium in conjunction with an 'on-axis' far-field aperture. The same solutions apply if a lens placed after the nonlinear medium focuses the phase-shifted beam onto an aperture near its focal plane (see figure 1a). At low beam powers virtually all of the energy is transmitted through the aperture, while at higher powers a large part of the energy is absorbed by the intercepting screen. If the nonlinear refractive coefficient, n_2, is positive, external self-focusing (Kaplan [4]) occurs and the principal focal spot is shifted towards the incoming beam. Self-defocusing takes place if n_2 is negative, and the diffraction focus is shifted to the far side of the linear focal plane.

A modification of the above arrangement focuses the radiation to a spot within the nonlinear medium with a second linear lens (depicted in figure 1b), thereby providing maximum intensity for the generation of nonlinear processes. Both continuous and pulsed radiation can be limited; in the latter case the external focal spot performs a rapid 'whiplash' motion towards the nonlinear medium as the pulse moves through the medium. Boggess et al [5] have achieved power limiting of 50 psec Nd:YAG pulses at 1.064 μm with such a system, using silicon as the nonlinear medium. The mechanism in this case is irradiance-dependent defocusing. Soileau et al [6-9] employed a similar experimental arrangement to achieve power limiting of 1.064 and 0.532 μm ultrashort pulses using liquid CS_2 as the medium. In these experiments, however, the nonlinear processes were only generated when the laser power P_i exceeded the self-trapping threshold power for the liquid.

In another modification, which is yet to be explored and tested experimentally, a second aperture is placed at the focal position in the nonlinear medium. This can perform several functions, for example it can act as an efficient spatial filter, or can be of use where an input beam is off-axis or for an input profile consisting of a large number of small spots.

2. CALCULATIONS

2.1 General

The important features in the diffraction pattern arising from the useful arrangement in fig. 1b are also produced by the simpler system shown in Fig. 1a. Hence it is instructive to study the model of external self-focusing by the simpler optical arrangement depicted in fig. 1a (see references to the theory [10,11]). The method of calculation is similar to that employed for aberration calculations near the focal plane of a linear lens [12]. The normalised intensity distribution of a beam of initial width w_0 aberrated by a thin nonlinear layer (thickness L) has been shown (Hermann, [10]) to be proportional to z^{-2} in the vicinity of the low-power focus, with

$$I(\rho;\psi,\phi) = \left| \int_0^\infty F(x) J_0(\psi x) \exp\left\{ i[\rho F(x)^2 - \phi x^2] \right\} . x \, dx \right|^2 \qquad (1)$$

where the following definitions apply:

(a) The focal length z has been scaled according to $\zeta = z/R_d$, where $R_d = \frac{1}{2} k_0 w_0^2$ is the diffraction length and k_0 is the wavenumber of the incident radiation.

(b) The radial coordinate in the far field, r, has been conveniently scaled as $\psi = 2r/(w_0 \zeta)$.

(c) The radial coordinate at the medium, r', has been scaled as $x = r'/w_0$, and F(x) is the shape of the transverse profile of the incident field amplitude.

(d) The spatial coordinate representing displacement from the linear (low-power) focal plane in the axial direction, y, has been scaled as $\phi = y R_d/z^2$.

(e) The nonlinear coefficient , which has been defined in reference 10, can be regarded as a parameter in the present model. It can be written as $\rho = \nu P_1/P_1$, where ν is a beam-shape parameter which measures the transverse spread of the incident beam and P_1 is a scaling power given by (see ref. 10) $P_1 = \pi n_0 w_0^2 \alpha_1 \{1 - \exp(-\alpha_1 L) k_0 n_2\}^{-1}$. Here, α_1 is the linear absorption coefficient and n_0, n_2 are the linear and nonlinear refractive indices respectively. The coefficient ρ is an intensity-dependent quantity.

(g) $J_0(\psi x)$ is the zero-order Bessel function.

Note that the intensity of the diffracted beam has been scaled to the maximum input intensity, so that I remains finite even when $\rho = 0$. The displacement coordinate ϕ has been formed with due allowance (to lowest order) for the effect of a linear lens upon the phase of the optical field. From Fourier optics it is known that the field is altered by a phase factor $\exp(ix^2/\ )$.

The amplitude function F(x) can be expanded for a single radially-symmetric spot as a power series of the form

$$F(x) = 1 - x^2 + bx^4 + \ldots \qquad (2)$$

Substituting equation (2) into equation (1) gives

$$I(\rho;\psi,\phi) = \left| \int_0^\infty F(x)\ J_0(\psi x)\ \exp.\left\{i(\rho(1 + 2b)x^4 - (2\rho + \phi)x^2)\right\}.x\ dx \right|^2 \qquad (3)$$

which displays a power-dependent displacement of the various profile features towards the focusing system. This type of behaviour represents an application of the 'displacement theorem' (reference [12], p 462). Furthermore, there is a power-dependent modification to the phase, which is at least of the fourth degree in x, producing in turn a power-dependent aberration of the various profile features.

The sign of determines whether the system is self-focusing (positive) or self-defocusing (negative). Equation (1) reveals that changing the sign of ρ is equivalent to reflecting the intensity distribution about the linear focal plane, ie.,

$$I(-\rho;\psi,\phi) = I(\rho;\psi,-\phi) \qquad (4)$$

The defocusing calculation is therefore equivalent to the self-focusing calculation, if the spatial domain is restricted to the region of the linear focal plane.

2.2 Single-mode input

We have integrated equation (1) numerically for different laser input profiles and have plotted the normalised intensity distribution in the region of the linear focal plane as a function of ψ,ϕ. The integration was performed with the use of adaptive routines which used both Gauss 10-point and Konrod 21-point rules [13]. The numerical accuracy of the integration technique was predetermined to be 10^{-5}, a level considered to be satisfactory, and as an additional check on the overall accuracy, the transmitted laser power for a nonabsorbing system was calculated in the linear focal plane and was found to be conserved to better than one percent. The results are depicted in figures 2 and 3 for single-spot profiles, with gaussian and parabolic shapes respectively, and with increasing positive values of ρ. In the gaussian case, the shape of the focal spot in the limit $\rho \to 0$ is easily calculated as

$$I(0;\psi,\phi) = \tfrac{1}{4}(1 + \phi^2)^{-1}\ \exp\left\{-\tfrac{1}{2}\psi^2/(1 + \phi^2)\right\}, \qquad (5)$$

which displays a gaussian shape transversely and a lorentzian shape axially. For increasing ρ the focal region stretches out along the optic axis, and its centre moves away from the linear focal plane. Furthermore, side peaks develop and grow as ρ increases, and eventually the focal ridge itself develops into a sequence of peaks, or bright spots. It is possible to evaluate the diffraction integral on-axis in terms of a confluent hypergeometric function (which also can be represented in terms of generalised Fresnel integrals) [14]:

$$I(\rho;0,\phi) = \tfrac{1}{4}(1+\phi^2)^{-1} \cdot \left| {}_1F_1(1, \tfrac{1}{2}(i\phi+3); -i\rho) \right|^2. \qquad (6)$$

Note that the property given by eqn (4) is also implicit in eqn (6). This on-axis formula possesses the property that the lorentzian shape becomes multiply peaked as ρ increases from zero. Similar structures associated with lens aberrations [15] have been held responsible for effects produced during laser-induced breakdown in gases [16], such as separated regions of intense ionization along the optic axis near the lens focus.

It is also apparent from figures 2a-c that the intensity along the optic axis declines rapidly beyond the linear focal plane, suggesting that for the purpose of maximising the power-limiting capability of a real self-focusing device it is desirable to position an aperture slightly beyond the linear focal plane (or before that plane for a defocusing device). In the experiments reported by reference 3 it was found that the largest intensity peaks, in the far-field profile generated by a gaussian-like input with a defocusing medium, can reside in the wings of the profile when ρ is large enough. This behaviour has been observed also in the present calculations if the plane of observation is positioned before the linear focal plane. At the focal plane, the insertion of a precisely gaussian input profile into the diffraction integral leads to diffraction patterns in which the largest peak is always on-axis [10]. This suggests that the input profiles claimed in reference 3 might not have been truly gaussian, but truncated gaussians, for which the higher-order terms are different. Noteworthy in this connexion is the observation that incident laser beams possessing field amplitudes of parabolic cross-section behave somewhat differently in the present model to those with precisely gaussian profiles; in the parabolic case the features along the optic axis all translate together with respect to increasing ρ. Hence, for large enough ρ, any plane cutting the optic axis perpendicularly in the neighbourhood of the linear focal plane intercepts an intensity profile with peak maxima in the wings, rather than on-axis. Further experimental work is evidently desirable so that these two explanations for the shift of power away from the axis to the wings can be satisfactorily disentangled, and also to establish the relevance of higher-order effects (represented by the wings of the beam) to the qualitative features of the diffraction pattern.

2.3 Higher-mode input

More complicated behaviour has been found with models in which the laser input profile takes the form of a symmetric spot surrounded by one or more concentric rings, or of concentric rings without a central spot. The annular input profile given by $F(x) = 4x^2(1-x^2)$ with $0 \leq x \leq 1$ has been explored, and the focal distributions are shown in figures 4a,b,c. In this

case there is a focal distribution on both sides of the linear focal plane; as ρ increases the focal region becomes elongated and attenuated, and internal peaks form. The number of peaks in the focal region increases, and the peaks move apart, as ρ increases. This combination of both self-focusing and self-defocusing occurs because the velocity of the electromagnetic wave within the nonlinear medium is diminished in regions of high intensity, so that a convex intensity profile renders the beam convergent while a concave profile produces divergent behaviour. Thus, an annular input beam traversing a nonlinear medium generates a wavefront with both converging and diverging characteristics, giving large peaks on each side of a linear focal plane. Note that amplitude profiles of the form $F(x) = ax^2 - bx^4 + \ldots$ possess a symmetric distribution along the optic axis with respect to the origin at the focal plane. The reason is evident from an analysis analogous to that used to obtain equation (3). Asymmetries appearing off-axis are attributable to terms of order x^4 and higher. Annular amplitudes which are odd in x will generally suffer displacement of the focal region (in proportion to ρ) as well as asymmetries along the optic axis.

2.4 Inclusion of nonlinear absorption

The extension of the above calculations to incorporate nonlinear absorption (below saturation) has been carried out, following the theoretical analysis of reference 10. Instead of equation (1), we now evaluate

$$I(\sigma,\beta;\psi,\phi) = \left| \int_0^\infty \frac{F(x)J_0(\psi x)}{\{1+F(x)^2\}^{1/2}} \exp.\left\{i[\sigma \ell n(1+\beta F(x)^2) - \phi x^2]\right\} x\, dx \right|^2 \qquad (7)$$

where σ is essentially the ratio of nonlinear refraction to nonlinear absorption coefficients, and β is the power parameter appropriately scaled. Note that β is also proportional to the nonlinear absorption coefficient. Changing the sign of n_2 (and therefore σ) is again equivalent to reflecting the intensity distribution given by equation (7) about the linear focal plane.

We have calculated the focal intensity distributions for a parabolic input ($F(x) = 1 - x^2$) with a fixed refraction parameter and several nonlinear absorption coefficients. The main feature to emerge from these calculations is the opposing behaviour of the absorptive and refractive mechanisms towards focal displacement. Where nonlinear absorption dominates, the diffraction focus remains at the linear focal plane, suitably attenuated in response to the magnitude of the nonlinear absorption coefficient. Where nonlinear refraction dominates, the diffraction focus is displaced from this plane to the maximum extent. This interplay between the two mechanisms explains many of the power-limiting features reported in reference 2 and the experimental results for the silicon switch reported in references [5].

3. DISCUSSION

The present model embraces both nonlinear refraction and absorption within the active medium. It adopts, for an effective dielectric susceptibility X of the medium, the expression

$$X(|E|^2) \propto k_0 + i\alpha_1 + (k_0 n_2/n_0 + i\alpha_2)\,|E|^2 \qquad (8)$$

where E is the envelope of the input field amplitude, and α_2 is the nonlinear absorption coefficient. Higher-order terms, and hence saturation effects, have been neglected. The model is generally inadequate for describing the interaction of pulsed radiation with materials whose refractive indices are strongly influenced by photogenerated free carriers (assuming, of course, that the pulse width does not exceed carrier lifetimes). Dynamic features have to be allowed for in these cases, and time-dependence must be admitted to the theoretical description both within the wave equation and through the time evolution of the free-carrier populations. Despite the absence of these features from the model, there is agreement for appropriate values of ϕ and ρ with the features reported in previous experimental work for both continuous radiation (middle IR) and pulsed radiation (near IR). Theoretical work giving more detailed quantitative predictions will await the development of satisfactory dynamic models for absorption and refraction (a) by laser-generated plasmas within liquids, and (b) for multiphoton and free-carrier effects within solid media.

Saturation (or partial saturation) of the nonlinear absorption is likely at higher laser powers. Recent research by Hill et al [16] with a gaussian beam at wavelength 10.6 μm traversing a crystal of cadmium mercury telluride at $175^{\circ}K$ has shown a nonlinear refractive index change $\Delta n = -7 \times 10^{-3}\, I^{1/3}$ where $I \propto |E|^2$ is the incident intensity in W/cm^2. The $I^{1/3}$ dependence reflects the important role of Auger recombination (see references in [16]) in limiting the saturation of absorption at the band edge, and similar behaviour can be expected with other materials such as indium antimonide. The optical model that has been explored by these authors differs from ours in that they constrain the nonlinear medium with a circular aperture, and also by their imposition of a quadratic approximation in the description of the phase profile. The latter simplification has been justified by them on the basis that saturation effects broaden the phase profile relative to the intensity profile. It is of interest to extend eqn. (6) for the gaussian-input profile and an infinite aperture, by suitably incorporating a new parameter μ, to account for saturation effects. Writing $\exp(-2x^2/\mu^2)$ for the phase profile, we find instead of eqn. (6):

$$I(\rho;0,\phi) = \frac{1}{4}\,(1+\phi^2)^{-1}\,\left|{}_1F_1\left(1,\ 1+\tfrac{1}{2}\,\mu^2(1+i\phi);\ -i\rho\right)\right|^2 \qquad (9)$$

The corresponding result restricted by the phase-profile approximation $\rho(1 - 2x^2/\mu^2)$ and by a finite circular aperture of radius $R(\leq\mu)$ is

$$I(\rho;0,\phi) = \left| \int_0^R \text{exp.} \left\{ -x^2(1 + i(\phi + 2\rho/\mu^2)) \right\} . \, x \, dx \right|^2$$

$$= [1 + (\phi + 2\rho/\mu^2)]^{-1} . \, e^{-R^2} . \left\{ \sinh^2(\tfrac{1}{2}R^2) + \sin^2 \tfrac{1}{2}R^2(\phi + 2\rho/\mu^2) \right\} \qquad (10)$$

The displacement of the diffraction focus (the tallest peak) is given by

$$\phi_{max} = - \, 2\rho/\mu^2,$$

as anticipated, and the remaining peaks within the focal region are symmetrically disposed. The intensity distribution, given by equation (9), exhibits pronounced asymmetry along the optic axis and is clearly shown in the numerical results in figs. 2a-c. Furthermore, eqns. (9) and (10) differ in the limit $\rho \to 0$, except when $R \to$. We conclude that great care should be taken with the mathematical modelling to ensure that effects associated with the tails of the beam and phase profiles are fully accounted for.

The range of validity in employing a quadratic approximation for the phase profile also can be tested by examining the case of parabolic input amplitude. Approximating the phase $\rho(1-x^2)^\lambda$, where $\lambda = 2/\mu^2$, by the first-order expression $\rho(1-2x^2/\mu^2)$, we have

$$I(\rho;0,\phi) = \left| \int_0^1 (1 - x^2) \, \text{exp.} \left\{ -i\theta x^2 \right\} x \, dx \right|^2$$

$$= \tfrac{1}{2} \theta^{-4} \left\{ 1 - \cos\theta - \theta \sin\theta + \tfrac{1}{2}\theta^2 \right\}, \qquad (11)$$

where $\theta = \phi + 2\rho/\mu^2$. Once again, there is symmetrical distribution about the peak at $\theta = 0$. The restriction to the lowest order* effect (displacement of the focal spot) is clearly a more serious source of error for input profiles possessing substantial tails.

In reference 10 the power-transfer curve (relating incident to transmitted power at the steady state) was calculated for a parabolic input profile. The latter shape was chosen by reason of the relative computational ease, compared to the gaussian. There is a large initial 'hump' on the parabolic transfer curve, whereas the corresponding gaussian curve exhibits a much less pronounced hump. This difference in behaviour reflects the different responses of the respective focal peaks towards increasing ρ. In order to inspect the origins of the difference most easily, we have drawn isophotes (lines of constant intensity) for the two cases in figs. 5-6. The displacement and aberration effects are clearly displayed. Cross-sections

---

* The term 'order' here refers to powers of x^2 in the series expansion for the optical phase profile, and should not be confused with the more general meaning of 'order' in optical aberration theory.

perpendicular to the optic axis are shown for the gaussian case in fig. 7, and reveal a substantial relative redistribution of radiant power away from the region of the optic axis as the intercepting plane crosses the linear focal plane. Another noticeable difference in behaviour between the two cases is that the focal ridge for the gaussian input remains 'anchored', with one end always extending as far as the linear focal plane, whereas for parabolic input all of the axial features translate together as ρ increases.

We have been able to effect a semi-quantitative comparison between theory and experiment, despite the absence of scaling information. The parameters relating to the 'far-field' experiment with indium antimonide reported in references 1-2 were inserted into our computer programme for evaluating eqn. (1), and intensity profiles were generated near the linear focal plane for various values of ϕ. It was found that the best fit could be obtained for three different values of ρ (specifically ρ = 2.20, 5.32, 8.72) if the observational plane intercepts the optic axis at ϕ = 0.6, and a typical result is shown in fig. 8. Issues relating to the shifting of radiant power away from the axial region should be unambiguously resolved by carrying out further experiments. For example, an experiment with an indium antimonide layer and material parameters corresponding to ρ = 10 appears feasible; the extent to which the present model with gaussian input (fig. 2b) describes this situation could be tested by performing spatial scans at various intercepting planes. Input profiles could also be varied, using transversely-graded filters (apodization).

The various types of behaviour described in section 2 are highly relevant to the performance and design characteristics of optical switches and power/energy limiters. Defocusing media such as Si, InSb and $Cd_xHg_{1-x}Te$ are generally preferable to focusing media, since in the latter cases the focal spot will rapidly move towards the focusing system, leading to a possibility of damage to the device rather than the reverse. Some of the advantages of this type of limiting device, when compared with other methods of limiting, are (1) complete passivity, (2) fast response and recovery times, (3) broadband operation, (4) absence of low-power optical filtering, (5) large dynamic range. Broadband operation is useful where the incoming radiation is of uncertain wavelength or where the laser is frequency-agile. Remaining problems which should be addressed in the future include

(1) Materials research directed to obtaining large values of n_2 and α_2,

(2) Production of high-quality media for imaging applications,

(3) Study of the effects of coherence quality of the beam (or pulses),

(4) Methods for minimising possible turbulence at low powers.

Lastly, the recent experimental and theoretical research by Khoo et al [18] and Khoo [19] on nonlinear refraction of a gaussian laser beam by a thin nematic liquid-crystal film has demonstrated both ringed structures in the far-field intensity distribution and strongly power-dependent oscillations along the optic axis. These features are in agreement with the predictions of our model, and lend support to the choice of refractive nonlinearity (quadratic in terms of the susceptibility, or cubic in terms of the macroscopic polarisation) where liquid crystal films are employed as the

nonlinear medium. Essential procedures for incorporating additional focusing, lenses, and mirrors into the model have been discussed in detail by these authors. The conversion from the model represented in fig. 1a to that shown in fig. 1b is relatively straightforward. Related work with self-phase modulation by nematic films also has been carried out very recently by Santamato and Shen [20]. However, it should be noted that despite their very large refractive nonlinearities, the present liquid-crystal systems appear to be far too slow to be considered for the purpose of limiting pulses of nanosecond or shorter duration.

4. ACKNOWLEDGEMENTS

The authors are grateful to colleagues at MRL for discussions and valuable suggestions on this topic, particularly Dr A.D. McLachlan, Dr J. Ternan, Dr B. Wendlandt, and Dr M. Brandt. Some of the material reported herein has already appeared in print in external publications [10,11,21,22].

5. REFERENCES

1. Miller, D.A.B., Mozolowski, M.H., Miller, A. and Smith, S.D., 1978, Optics Commun., 27, pp 133-136.

2. Weaire, D., Wherrett, B.S., Miller, D.A.B. and Smith, D.S., 1979, Optics Lett., 4, pp 331-333.

3. Miller, A., Miller, D.A.B. and Smith, D.S., 1981, Adv. Phys., 30, pp 697-800.

4. Kaplan, A.E., 1969, Radiophys. Quantum Electron., 12, pp 692-696.

5. Boggess, T.F., Moss, S.C., Boyd, I.W. and Smirl, A.L., 1984, Optics Letters 9, pp 291-5; see also Paper FS6, Technical Digest, CLEO 1984, Anaheim, California, pp 270-272.

6. Soileau, M.J., Franck, J.B. and Veatch, T.C., 1980, in Laser-Induced Damage in Optical Materials, Nat. Bur. Stand. Spec. Publn. No. 620, pp 385-393.

7. Soileau, M.J., Williams, W.E., Van Stryland, E.W. and Brown, S.F., 1981, in Laser-Induced Damage in Optical Materials, Nat. Bur. Stand. Spec. Publn. No. 638, pp 557-567.

8. Soileau, M.F., Williams, W.E. and Van Stryland, E.W., 1983, IEEE Jl. Quant. Electron., 19, pp 731-735.

9. Williams, W.E., Soileau, M.J. and Van Stryland, E.W., 1984, Optics Commun., 50, pp 256-260.

10. Hermann, J.A., 1984, J. Opt. Soc. Am. B. 1, pp 729-736.

11. Hermann, J.A. and Grigg, M.E., 1984, Optics Commun., 49, pp 367-370.

12. Born, M. and Wolf, E., 1973, Principles of Optics, 3rd Edition (London: Pergamon Press), Chs. 8 and 9.

13. Malcolm, M.A. and Simpson, R.B., 1976, A.C.M. Transactions of Mathematical Software 1, pp 129-146.

14. Abramowitz, M. and Stegun, I. (Eds.), 1968, Handbook of Mathematical Functions, 5th Edition (New York, Dover) pp 262, 503.

15. Aaron, J.M., Ireland, C.L.M. and Grey Morgan, C., 1974, J. Phys. D: Appl. Phys. 7, pp 1970-1978.

16. Evans, L.R. and Grey Morgan, C., 1969, Phys. Rev. Letters, 22, (21) pp 1099-1107, and references therein.

17. Hill, J.R., Parry, G. and Miller, A., 1982, Optics Commun., 43, pp 151-156.

18. Khoo, I.C., Yan, P.Y., Liu, T.H., Shepard, S. and Hou, J.Y., 1984, Phys. Rev. A, 29, pp 2756-2764.

19. Khoo, I.C., 1982, Appl. Phys. Lett., 41, pp 909-911.

20. Santamato, E. and Shen, Y.R., 1984, Optics Letters, 9, pp 564-566.

21. Hermann, J.A. and Kennett, S.R., 1985, Optics Communications, 54, pp 47-53.

22. Hermann, J.A., 1985, Optica Acta, 32, pp 541-547.

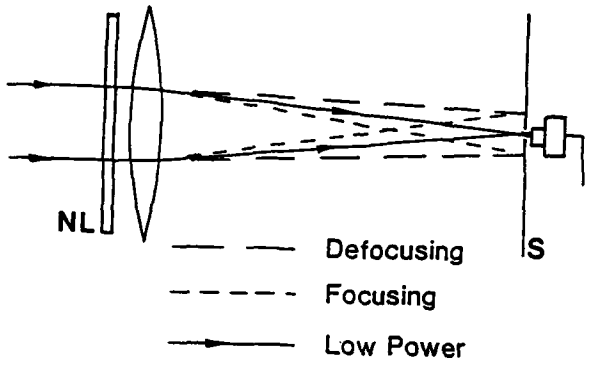

(a)

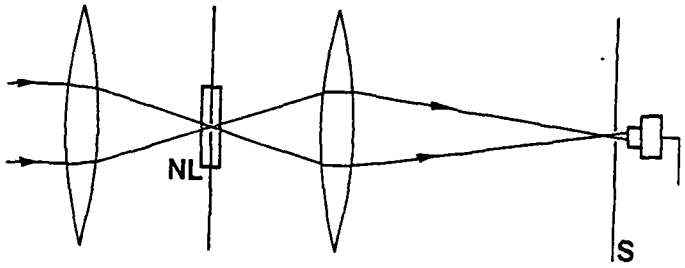

(b)

FIGURE 1 *Arrangement for a self-focusing/defocusing power limiter:* (a) simple model, (b) practical model. The nonlinear medium is designated NL, and the screen S.

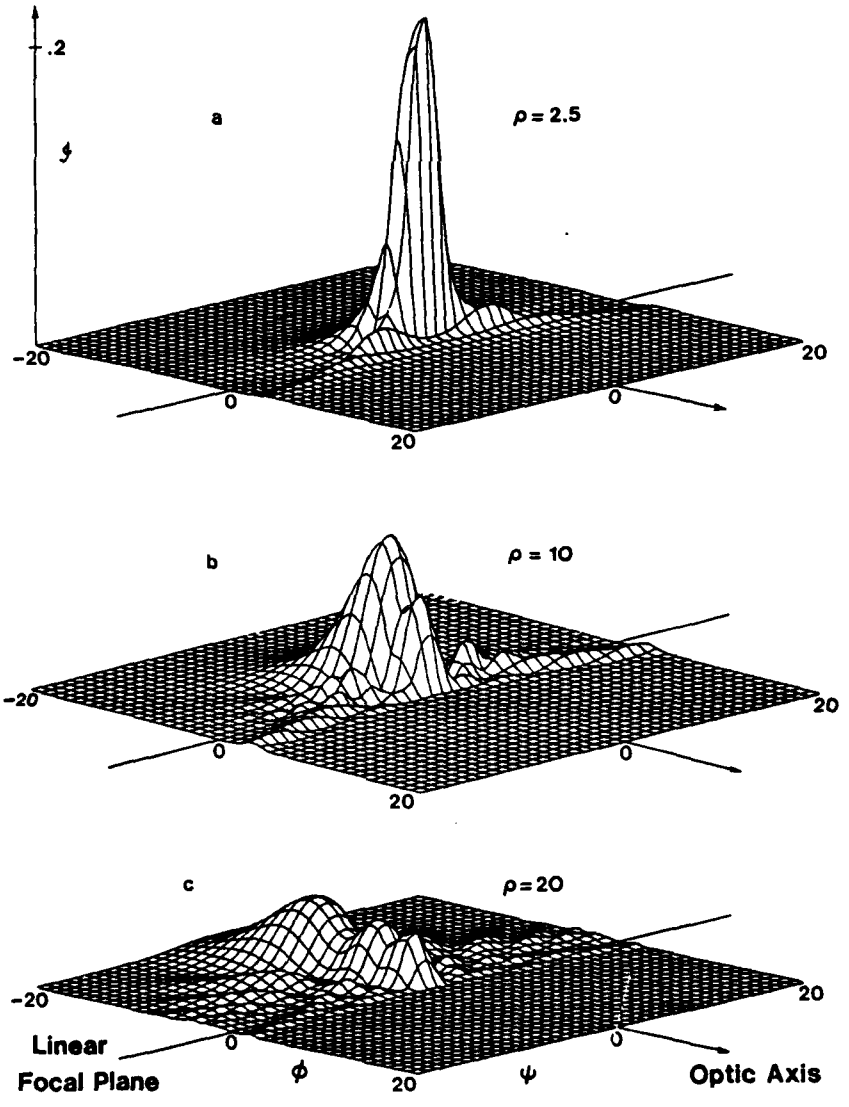

FIGURE 2 Normalised intensity distribution for the gaussian input $F(x) = \exp(-x^2)$ in the region of the linear focal plane. Radiation is incident from the left for self-focusing media and from the right for self-defocusing media. Fig. (d) is a close-up of Fig. (c) with an expanded scale.

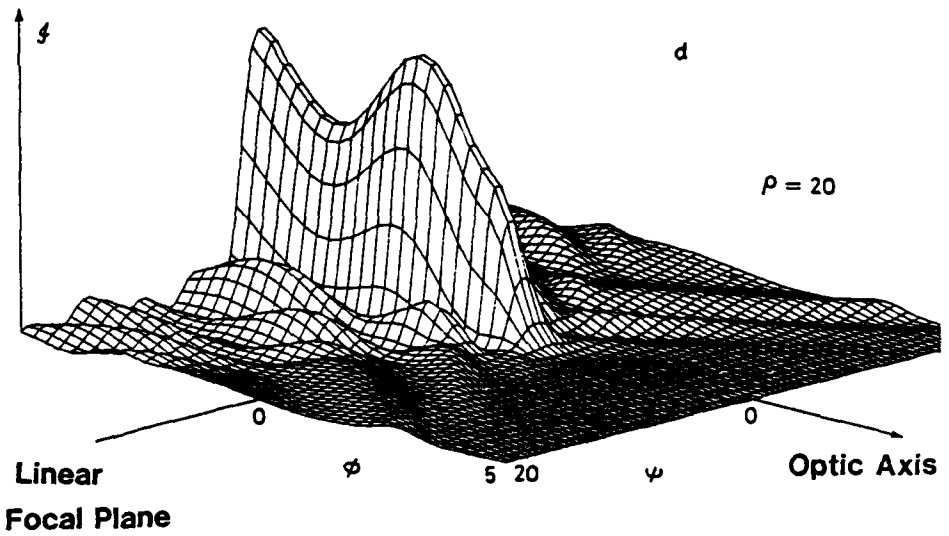
$\mathcal{I}$
d
$\rho = 20$
0
0
ϕ
5 20
ψ
Linear
Focal Plane
Optic Axis

FIGURE 2(d)

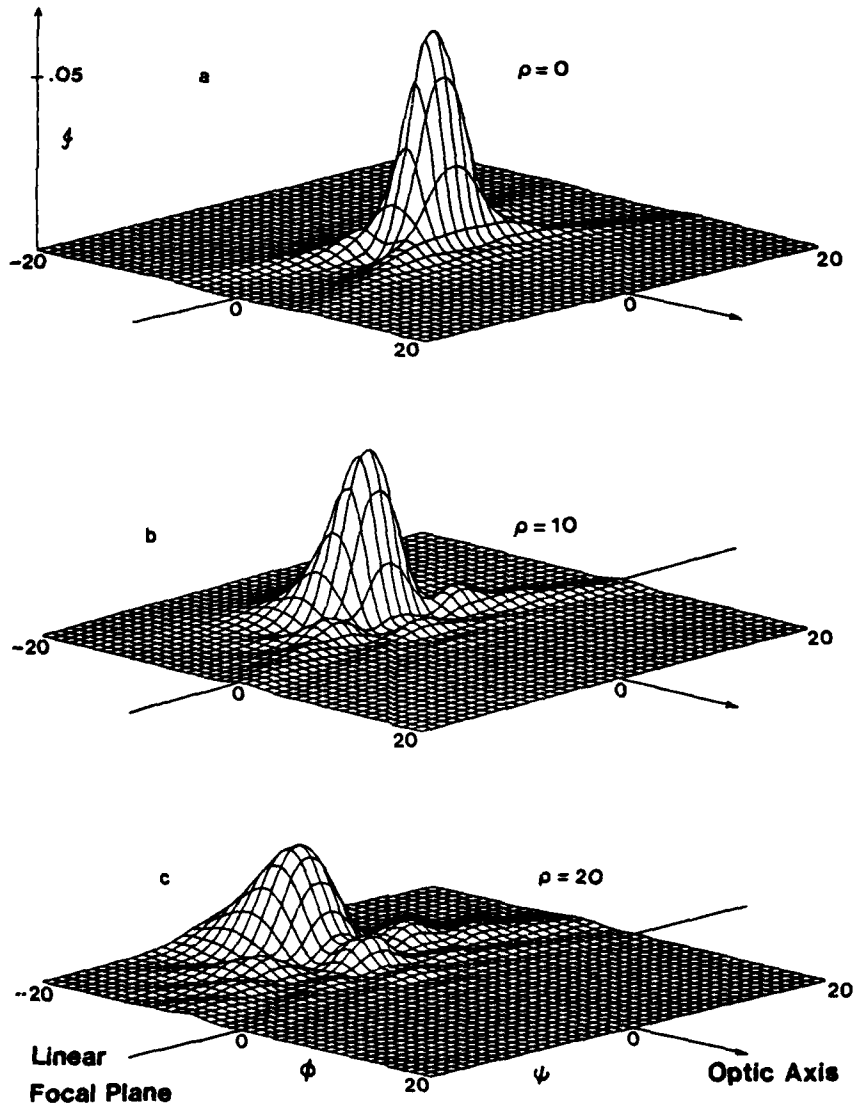

FIGURE 3 Normalised intensity distribution for the parabolic input amplitude $F(x) = 1 - x^2$.

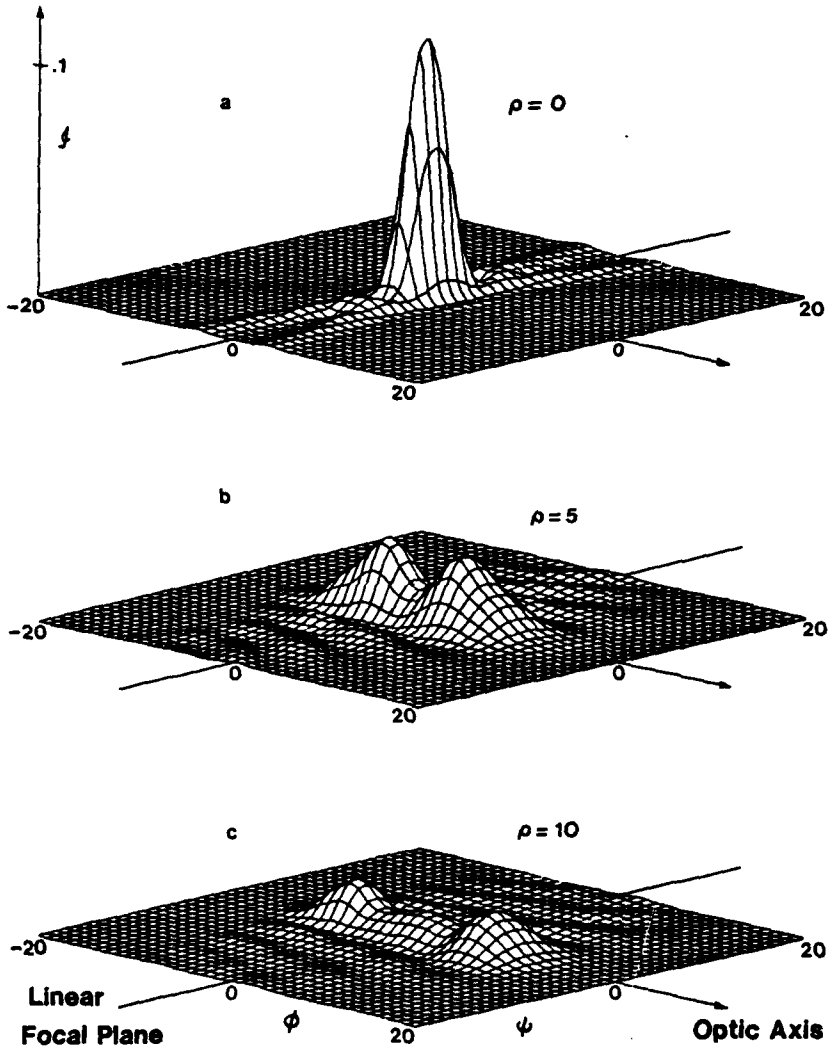

FIGURE 4 Normalised intensity distribution for the doughnut-shaped input amplitude $F(x) = 4x^2 (1 - x^2)$.

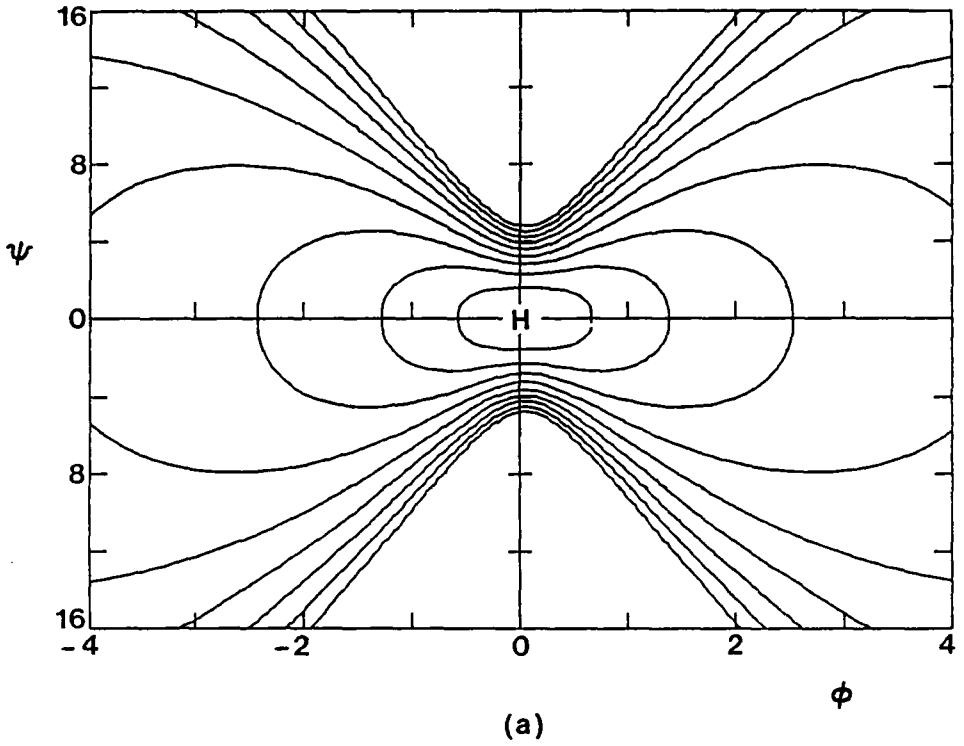

FIGURE 5 Isophotes near the linear focal plane, for gaussian input amplitude; (a) $\rho = 0$, (b) $\rho = 5$. Intensity maxima are designated H and minima L. Contour intervals are half orders of magnitude; the highest contour in (a) is $10^{-1/2}$ and in (b) is 10^{-1}.

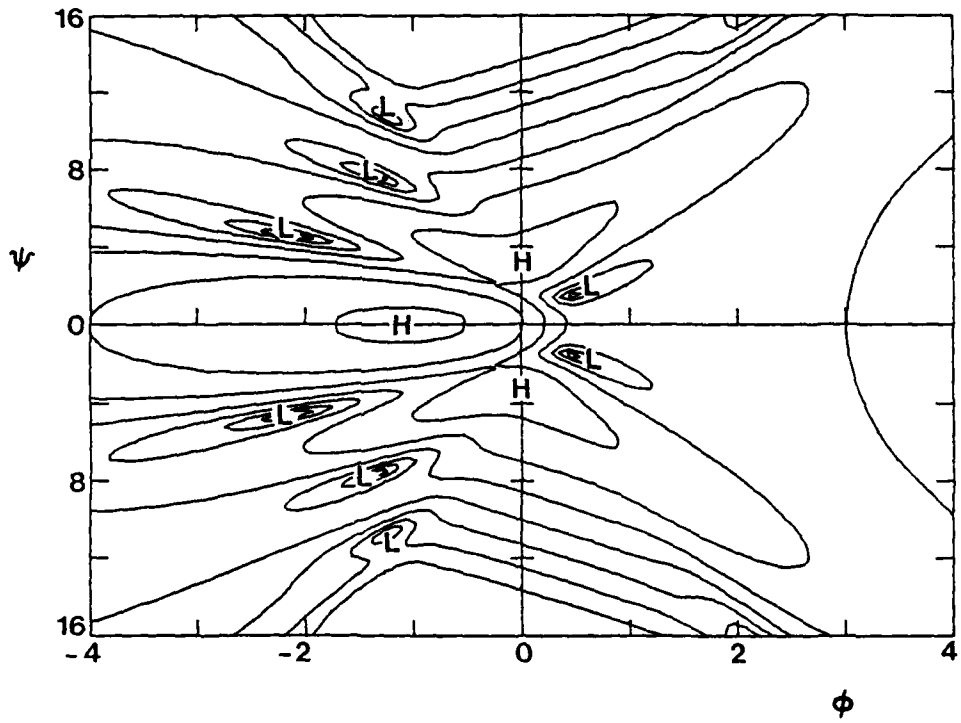

(b)

FIGURE 5(b)

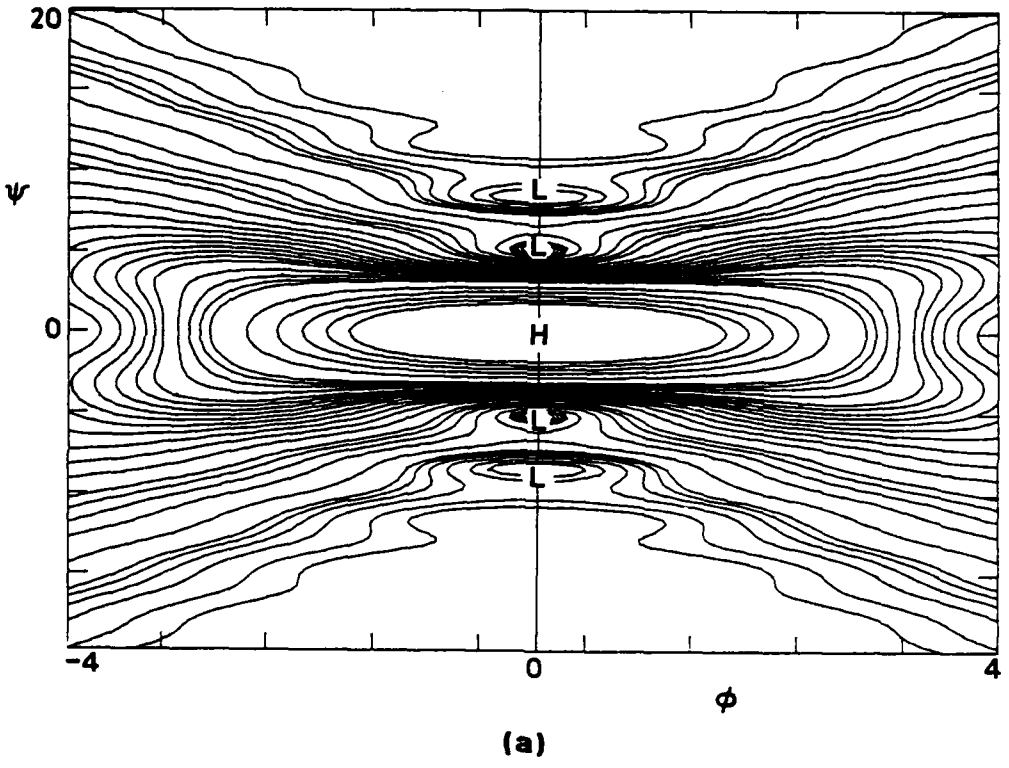

FIGURE 6 Isophotes near the linear focal plane, for parabolic input amplitude; (a) $\rho = 0$, (b) $\rho = 5.0$, (c) $\rho = 10$. Maxima are designated H and minima L. Contour intervals are spaced on a semi-log scale with ten equal divisions per order of magnitude.

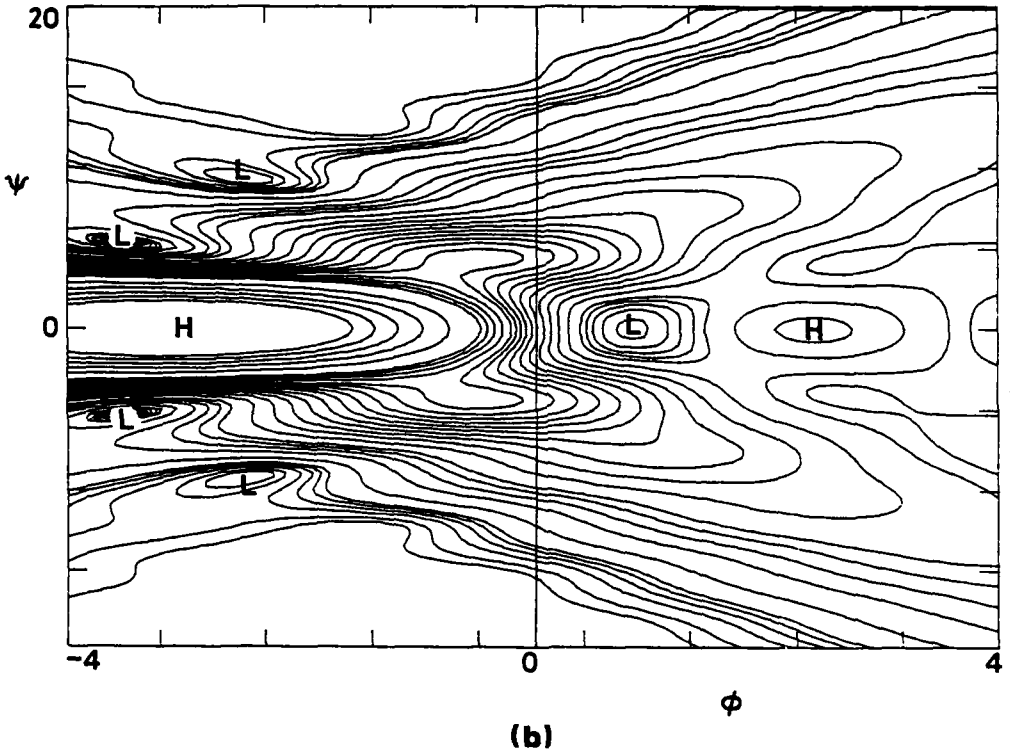

(b)

FIGURE 6(b)

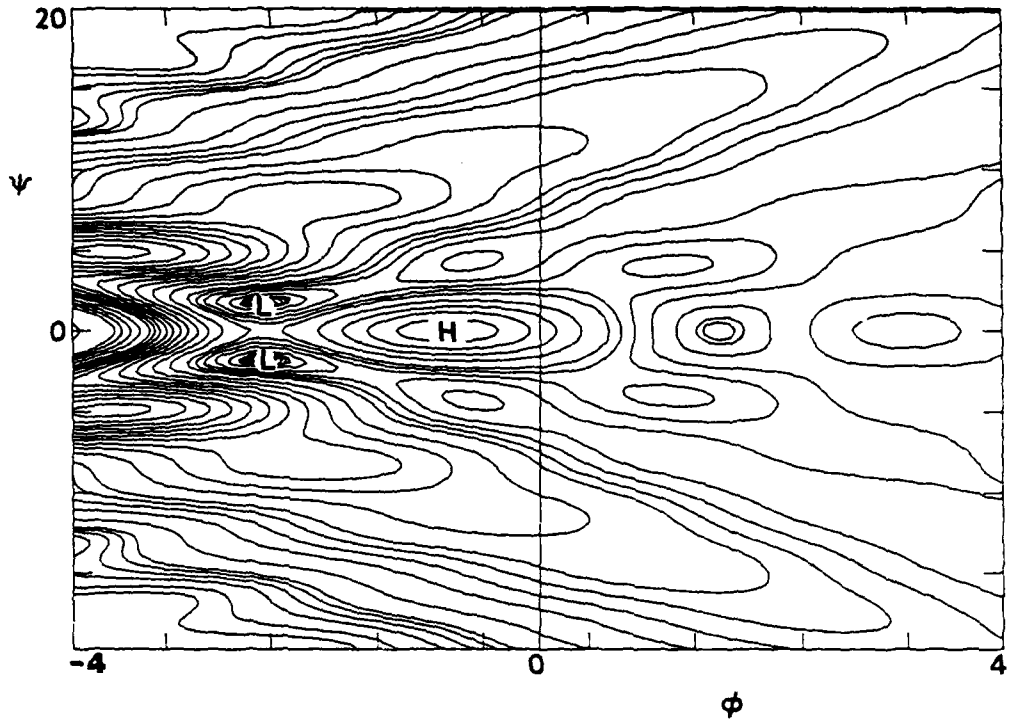

(c)

FIGURE 6(c)

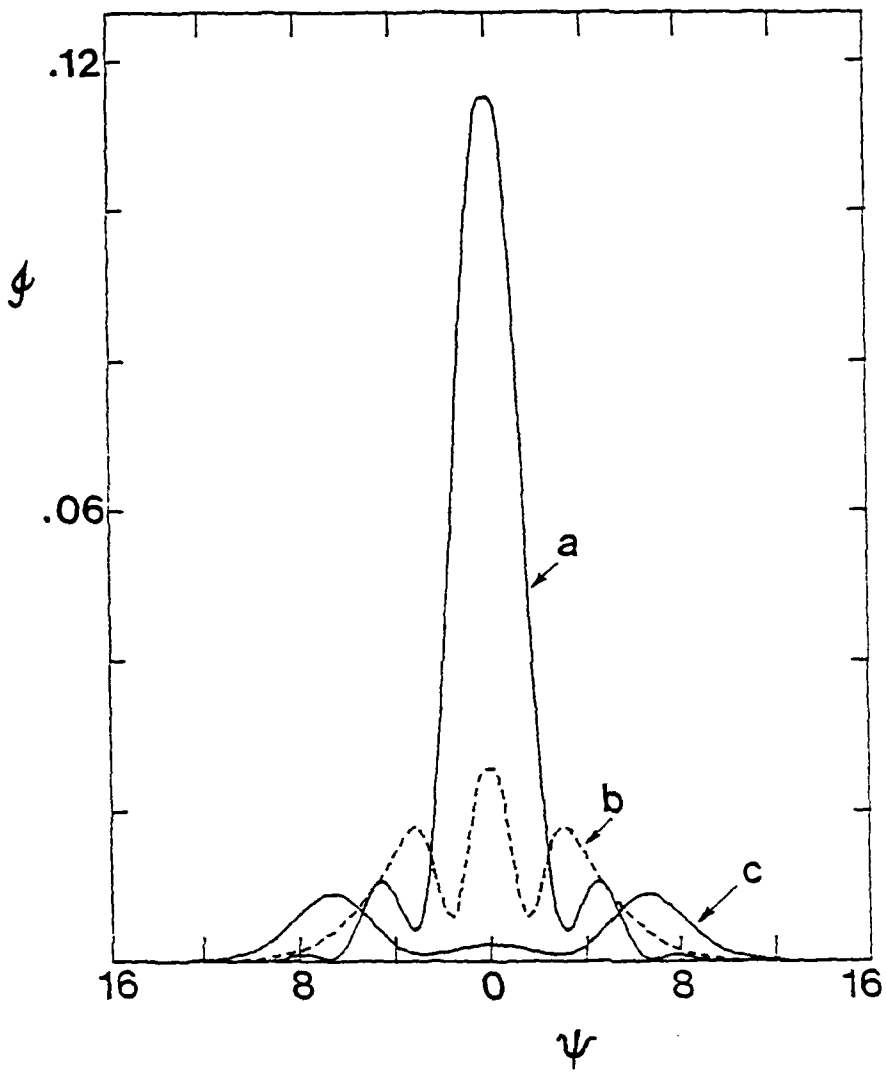

FIGURE 7 Intensity profile cross-sections for gaussian input, with $\rho = 5$; (b) $\rho = -1$, (b) $\phi = 0$, (c) $\phi = 1$.

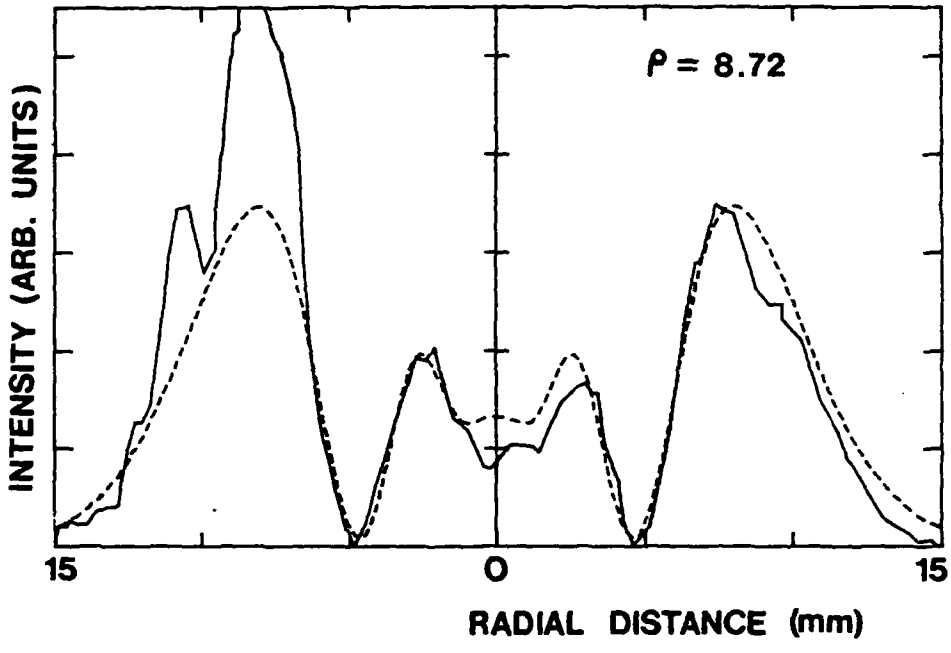

FIGURE 8 Transverse profile for gaussian input at $\rho = 8.72$: (a) Full line, experimental (ref. 1); (b) Broken line, theoretical matched at $\phi = 0.6$.

END

DATE
FILMED

2-87